Application of Machine Learning to Lightning Strike Probability Estimation

Aderibigbe Adekitan
Group for Lightning and Overvoltage Protection
Technische Universitaet Ilmenau,
Ilmenau, Germany
aderibigbe-israel.adekitan@tu-ilmenau.de

Michael Rock
Group for Lightning and Overvoltage Protection
Technische Universitaet Ilmenau,
Ilmenau, Germany
michael.rock@tu-ilmenau.de

2020 International Conference on Electrical Engineering and Informatics (ICELTICs) | 978-1-7281-8199-8/20/$31.00 ©2020 IEEE | DOI: 10.1109/ICELTICS50595.2020.9315398

***Abstract*—The risk of a lightning strike to a structure is influenced by geometry, the type of material of the structure, and proximity to other structures. The probability of lightning strike to different points on an object can be determined by applying the concept of probability modulated collection volume using the dynamic electro-geometrical model (DEGM). The numerical computation of the DEGM is computer resource-intensive and requires extensive programming and analysis to implement, which may be difficult to apply by engineers setting up lightning protection systems in the field. This study explores the feasibility of applying an artificial neural network (ANN) using a network with 18 hidden neurons and the Levenberg-Marquardt algorithm for training the model. The strike probability predictions by the neural network give close values to the numerical results. The ANN approach is further supported by predictive equation-based models developed using data pattern recognition and curve fitting techniques, as easy to use alternatives to the numerical DEGM simulations. The ANN model had an overall regression R^2 of 1, and it performed better than the equation-based model.**

Keywords—dynamic electro-geometrical model, interception efficiency, lightning current distribution, lightning protection system, artificial neural network, pattern recognition

I. INTRODUCTION

Lightning is the discharge of transient, high energy current in the atmosphere. A complete discharge is known as a lightning flash, while a discharge that involves objects on earth may be referred to as a lightning strike. The lightning discharge process entails the downward movement of charges referred to as a downward leader via random conducting paths, from the cloud charge centres towards the ground. This is followed by an upward leader and then an upward return stroke, from the ground towards the cloud. Ultimately, this neutralizes the charges in the leader channel. Lightning discharge can be of negative or positive polarity, and less than 10% of all cloud-to-ground discharges are of the positive type, with directly measured current peaks of up to 300 kA already documented [1].

Protecting structures on earth against lightning strikes requires an in-depth understanding of how a structure is exposed to lightning strike relative to other nearby structures. The concept of lightning collection volume explains the associated strike risk for an object, and the extent of protection offered by any lightning protection system can also be estimated by considering the limit of its protection zone [2]. Damage to structures and sensitive equipment and injury to persons as a result of lightning strikes, and in some cases lightning-induced fires are usually due to lack of lightning protection on such structures, or as a result of poor design of such protection systems.

Striking distance is a term that reflects the extent in terms of geometric distance, from which a point on a structure is exposed to downward leaders and may be struck by lightning [3]. This has been used over time to estimate the protection zone of a lightning rod. The rolling sphere method assumes that the probability of a strike to all points on a structure is the same, and it does not differentiate between strikes to ground, rods and transmission lines as validated by experimental analysis, which further provided insights on the effects of charge polarity on strike risk [2, 4]. A structure is deemed protected from lightning strikes using the rolling sphere concept if no point on the structure is touched by a sphere of a fixed radius corresponding to a specific protection level [5]. The rolling sphere must only touch lightning rods and the ground [6]. This analysis does not help in identifying high-risk points on the structure, as all points on the structure are assumed to be equally at risk by the rolling sphere concept.

The dynamic electro-geometrical model (DEGM) is a concept for evaluating the probability of a lightning strike to a structure, on a point-by-point basis. By creating meshes on a structure of interest, the probability of strike to different points on the meshed structure can be determined using several rolling sphere radii, unlike the rolling sphere concept that is based on a fixed radius. The DEGM concept can be deployed using numerical techniques that involve extensive programming and computation time. Although the DEGM provides more information for a better design of lightning protection systems for an object, performing the DEGM analysis may be a major challenge due to the intricate level of programming, and computer resources required as several iterations are performed, which may take several hours to compute even on advanced simulation computers.

This study investigates the feasibility of developing models for applying the dynamic electro-geometrical model to a structure without the need for repetitive extensive numerical simulations. To achieve this, recent trends based on knowledge discovery from datasets were considered by applying machine-learning techniques; specifically, the artificial neural network (ANN) and a data fitting technique were applied to recognize patterns within the dataset. Firstly, numerical computation of the DEGM to a cuboid structure as a case study was performed

978-1-7281-8199-8/20/$31.00 ©2020 IEEE

using various dimensions, and the dataset accumulated from these simulations were studied for evolving alternative approaches to the numerical simulation. ANN enables fast and accurate computation of predictive models and has been applied in lightning detection studies [7]. ANN mimic the biological neural workings of the human brain for evolving solutions, by adjusting the weights of artificial neurons in order to fit its output to target values based on given inputs, as a mimic of the biological stimuli process.

II. The Concept of the DEGM

Applying DEGM to determine the probability of a lightning strike to points on an object involves a number of stages. For a cuboid structure as considered in this study, the surface of the cuboid is meshed into several points at equal spacing, thereby generating several surface points on the structure to which a lightning downward leader may attach. Also, since downward leaders descend towards the structure from above, spaces around, and above the cuboid within the lightning collection volume of the structure are also meshed into multiple space points from which lightning can be oriented towards the object as shown in Fig. 1. For each space point, the nearest surface point(s) on the structure or ground, in terms of geometric distance is determined as the likely strike point for any downward leader orientating from that specific point in space, either from above or the side of the structure [8]. The effective striking distance for each struck surface point is converted to a probability value by using the lightning probability density function [9]. The cumulated probability of a lightning strike for each surface point is finally converted to a percentage of the total for the structure.

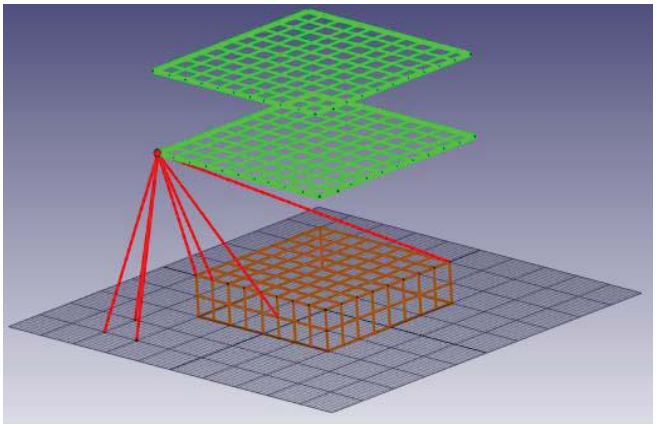

Fig. 1. Illustration of meshed space points above, and surface points on the cuboid structure

III. The ANN Model

The Artificial Neural Network (ANN) is a computational learning model that mimics the functioning of the neurons of the central nervous system of the mammalian brain. The ANN has artificial neurons called nodes, which can be used for evaluating a function based on given inputs, in order to produce a corresponding output. The nodes are usually interconnected and structured in layers referred to as hidden layers. From the input layer, the output of one neuron will become the input of the next neuron until the final output stage. The input variables are supplied to the input layer, and this is transmitted to the interconnected neurons in stages for processing, and the final output is sent to the output layer. The output of each node is triggered when the weighted input sum is processed by a preset activation function (transfer function) which is usually non-linear. This gives an output which is equivalent to an electrical potential in biological systems [10]. The neurons are interconnected by paths with a given weight value (W), and the weight of each path can be adjusted by a learning algorithm that tries to find the best weight value for each path in the model in order to accurately define the output values based on the set of inputs [11]. The ANN learning process can be supervised, unsupervised or the hybrid mode, and it is very efficient for modelling non-linear systems.

A basic model of an artificial neuron is shown in Fig. 2. ANN has been applied in different fields of study. ANN has been used for forecasting, prediction, and data classification [12], optimization [13], maintenance data analysis [14], load forecasting [15], educational data studies [11], climate studies [16], etc.

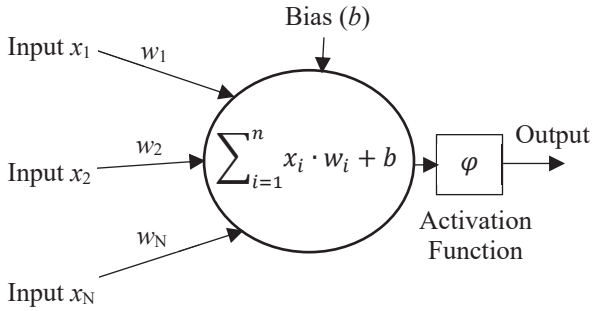

Fig. 2. A model of an artificial neuron

To achieve an ANN-based DEGM; a 7-input neural network model was developed using a two-layer feed-forward network comprising of 18 neurons, as shown in Fig. 3. The dataset containing 36900 samples (e.g. A = 29.4618, B = 1, C = 12, D = SW, E = 1600, F = 30, and G = 4800) was randomly divided into three in the ratio, 70% for training, 15% for performance evaluation, and the remaining 15% for testing. The model was trained using the Levenberg-Marquardt optimization algorithm for supervised learning using the backpropagation rule. The analysis was carried out using the neural fitting tool on MATLAB. The training process is performed iteratively by feeding the inputs, updating the neural weights, and getting an output repeatedly until a preset limit is attained. Each of this iteration is referred to as an epoch, and in this study, the iteration was terminated after 1000 epochs. The performance of the model was evaluated using the mean square error and regression R^2 values.

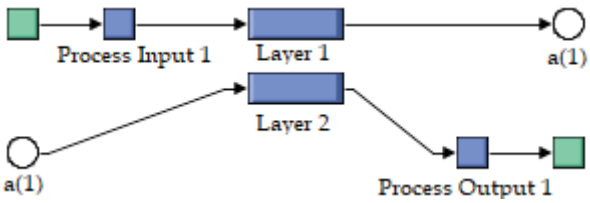

Fig. 3. ANN model for DEGM

IV. The Methodology

Two cuboids with different roof surface areas were considered and analyzed in this study. The first cuboid referred to as Cuboid A, has a roof area of 40 m by 40 m, while the second one, Cuboid B has a dimension of 50 m by 20 m as illustrated in Fig. 4. For the two cuboids, the following heights were considered, 10 m, 30 m, and 50 m as the major source of the dataset for the artificial neural network, and curve-fitting analysis. After developing a trained and validated ANN model on MATLAB, and equation-based models using ndCurveMaster [17] as a data fitting tool, the performance of the model, and the extent to which its predictions can be generalized is further tested. This was achieved using samples from a new dataset generated from Cuboid A, and Cuboid B of heights 20 m, and 40 m, which were not part of the initial dataset on which the model is based.

The dynamic electro-geometrical model was applied to Cuboid A, and B of various dimensions separately, and the probability of a strike in percentage, hereby referred to as the target was determined for each meshed points on the cuboid. The inputs and the output of a model must be well defined to apply machine-learning techniques to a dataset. In this case, the desired output is the target (i.e. the percentage probability of strike to each point) which has been determined by DEGM analysis. There is a need to define the input features as independent variables that will define the desired output. To do this, attributes of the cuboid and the DEGM as a concept were considered to generate seven input features, as defined in the following section.

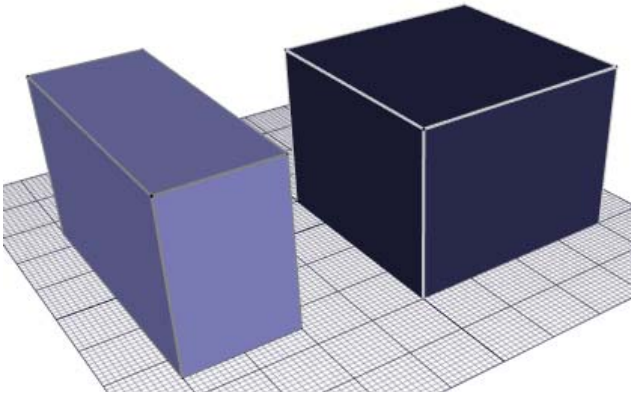

Fig. 4. Cuboid A and Cuboid B

Firstly, the surface points on the cuboid structure were classified into five different types: sidewall (SW), corner (C), wall edge (WE), inner roof (IR), and roof edge (RE). This nomenclature is illustrated in Fig. 5.

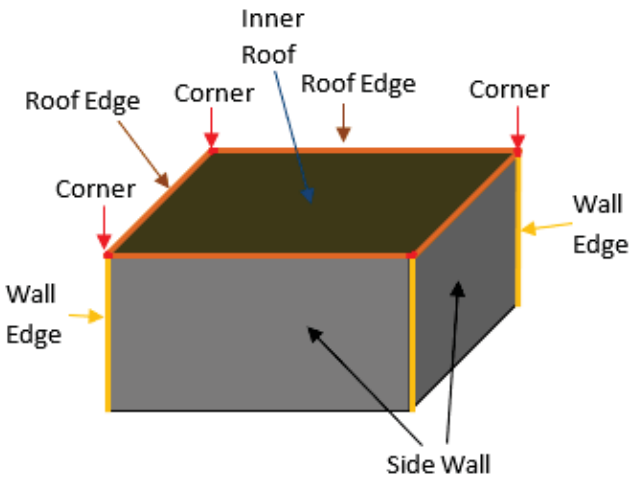

Fig. 5. Types of surface points on a cuboid structure

The seven input features are defined as follows:

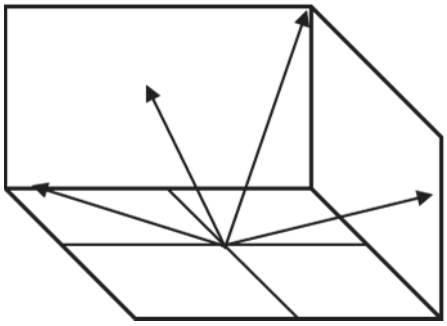

Fig. 6. Surface point's displacement from the datum point

- Feature A – This is the distance between each surface point and a reference point at the centre of the cuboid on the ground level, as illustrated in Fig. 6. This parameter measures the relative displacement of each surface point from the datum point.
- Feature B – This reflects the exposure of each type of surface points in angular terms using a single horizontal surface as a reference plane at each object height. For corners and wall edges, the exposure angle is 90°, while it is 1° for all other points. This concept is illustrated in Fig. 7.

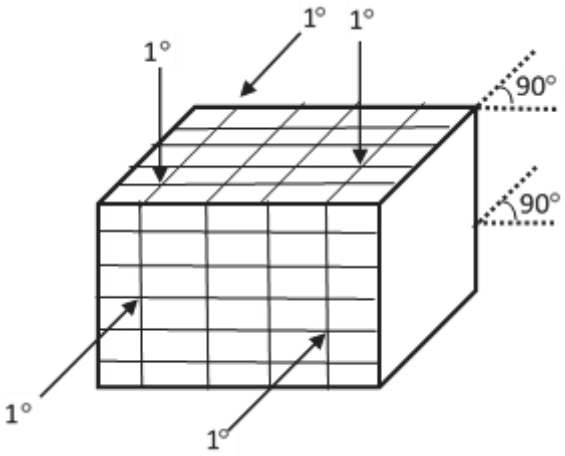

Fig. 7. The angular exposure of each surface point

- Feature C – The height of each discretized surface point above the ground, as illustrated in Fig. 8.

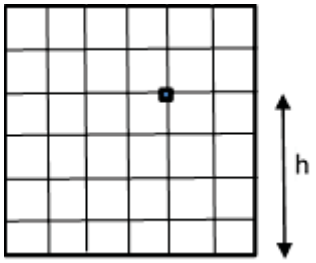

Fig. 8. The height of a cuboid surface point from the ground

- Feature D – The type of surface point coded as follows: 1 for the side wall (SW), 2 for the wall edge (WE), 3 for the corner (C), 4 for the roof edge (RE), and 5 for the inner roof (IR).
- Feature E – The surface area of the cuboid's roof (exposed top) in m^2.
- Feature F – The height of the cuboid.
- Feature G – The total surface area of the four cuboid sides in m^2.

V. RESULTS

A. ANN result

The ANN model was trained using the Levenberg-Marquardt algorithm, and the performance of the model will be discussed in this section. In order to prevent over-training, the model performs validation checks to ensure that the training errors is decreasing after each iteration, and if for six iterations, the validation error does not decrease during the validation checks, the training is terminated. For the 1000 epoch, there was no validation failure. The simulation (training, validation, and testing) was completed in 2 minutes. The training status of the ANN model after completion is shown in Fig. 9.

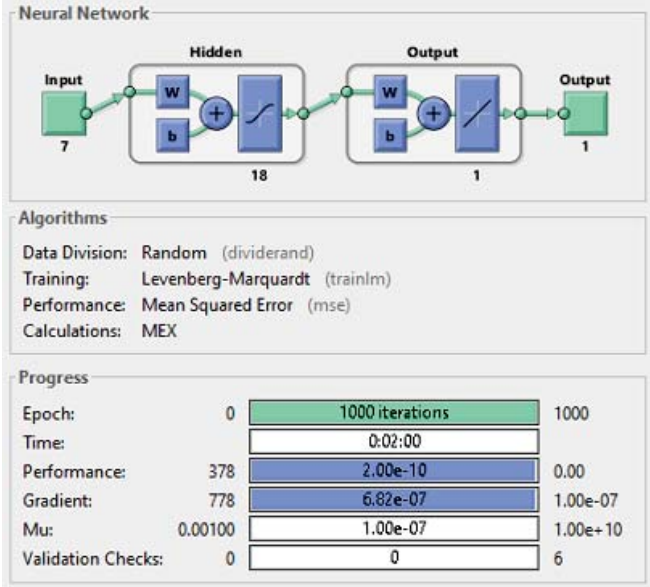

Fig. 9. The Artificial Neural Network and training progress report

The performance of the model can be evaluated in terms of the mean square error (MSE), and the regression R^2 value. The lower the MSE, the better the result and the higher the R^2 value, the better the model results. R^2 values are in the range from 0 to 1. For the training process, the MSE observed is 2.000×10^{-10}, 2.103×10^{-10} for validation, and 2.138×10^{-10} for the testing. The regression plots in Fig. 10 to Fig. 13 show the extent of the relationship between the predicted output and the actual expected output (percentage probability of lightning strike from DEGM), i.e. the target. Fig. 10 shows the regression plot for the training, Fig. 11 for the validation, Fig. 12 for the testing and Fig. 13 for the overall model performance. An overall R^2 value of 1 was achieved, which indicates a good model fit.

The performance validation in terms of the reduction of the MSE with successive iterations is shown in Fig. 14. Fig. 15 shows the error histogram. The error histogram is a plot of the error distribution, and it shows that highest error is around the central value of 5.09×10^{-6}, and the error decreases on both sides of the maximum error point, and this is a good indication of minimal predictive error. For an overview of the predictive ability of the ANN model, some samples of the predictions for Cuboid A, and Cuboid B from the five cuboid heights, i.e. 10 m, 20 m, 30 m, 40 m, 50 m are presented in Table I.

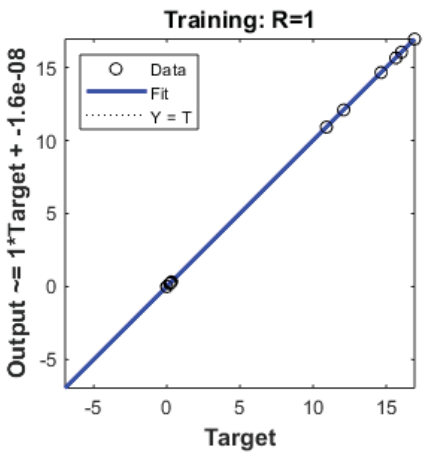

Fig. 10. Regression plot for the training data

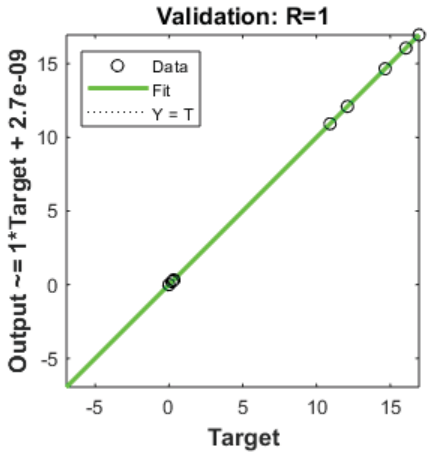

Fig. 11. Regression plot for the validation data

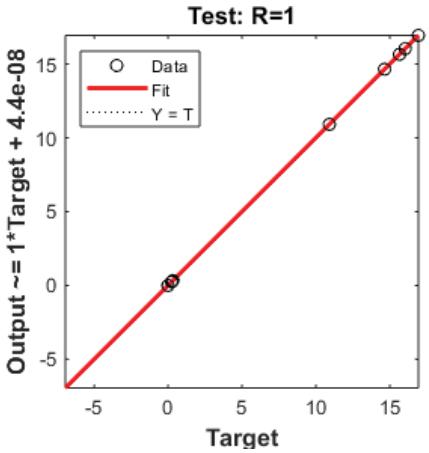

Fig. 12. Regression plot for the test data

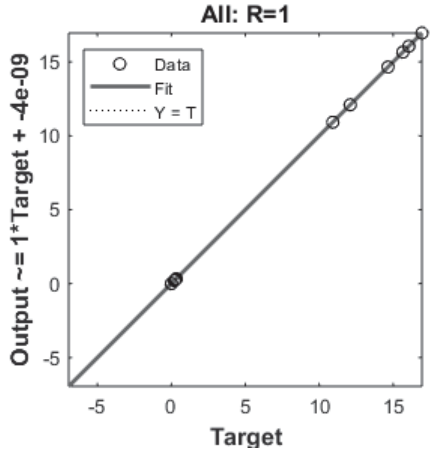

Fig. 13. Regression plot for the overall model

The results from serial number 1 to 18 in Table I are from samples used in the ANN model development, i.e. 10 m, 30 m, and 50 m. In order to evaluate the ability of the model to predict for new data, data samples from 20 m, and 40 m, both for Cuboid A and Cuboid B which were not part of the ANN model development process were analyzed, and the results for few samples are shown comparatively from serial number 19 to 30 in Table 1. Although the predictions are not perfect, the result shows a close approximation to the target, especially for the roof edge (RE), the internal roof (IR), and the corner (C) points.

B. Equation-based model results using data fitting

As an alternative to the ANN approach, the possibility of deploying equations that reasonably model the attributes of the dataset for predictive analysis was explored. Separate equations and analysis were developed for each type of surface point, i.e. WE, SW, RE, IR, and C, by exploring data fitting techniques using ndCurveMaster. The types of surface points are coded from 1 to 5, as previously defined. Only three key features were considered in the model, and these are feature A, feature C, and feature F. The addition of more features, only made the equations more complex without a significant improvement in accuracy. Unlike the analysis for ANN, where the percentage of the probability of lightning strike was directly predicted, for the first equation-based model the probability modulated collection volume (PMCV, i.e. summed probability value for each point) will be predicted, and this will be converted to a percentage at the end of the analysis.

TABLE I. COMPARISON OF THE PREDICTED RESULTS WITH THE TARGET VALUE

SN	Cuboid Type	Point Type	Target	ANN Prediction
1	A10	SW	0.00001	0.00002
2	A10	RE	0.29900	0.29893
3	A10	C	10.91782	10.91782
4	A30	IR	0.00288	0.00289
5	A30	RE	0.23580	0.23581
6	A30	C	14.65174	14.65174
7	A50	SW	0.00008	0.00008
8	A50	RE	0.20343	0.20340
9	A50	C	16.05324	16.05324
10	B10	IR	0.00705	0.00706

11	B10	RE	0.33125	0.33123
12	B10	C	12.09545	12.09545
13	B30	SW	0.00010	0.00011
14	B30	RE	0.25201	0.25202
15	B30	C	15.65919	15.65919
16	B50	C	16.94614	16.94614
17	B50	SW	0.00000	0.00000
18	B50	RE	0.21474	0.21474
19	A20	WE	0.00097	0.08164
20	A20	C	13.32972	13.22496
21	A20	RE	0.26071	0.26391
22	A40	SW	0.00007	-0.09099
23	A40	RE	0.21777	0.21473
24	A40	C	15.48832	15.52843
25	B20	C	14.41524	14.31642
26	B20	SW	0.00005	0.05884
27	B20	RE	0.28195	0.28757
28	B40	IR	0.00244	0.00436
29	B40	RE	0.23105	0.22936
30	B40	C	16.43327	16.46468

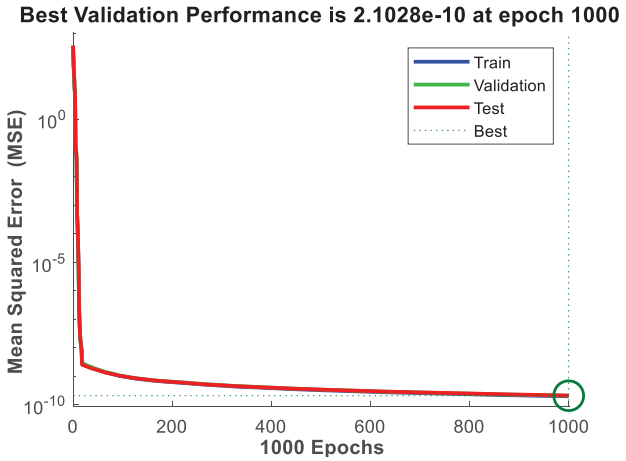

Fig. 14. MSE trend for the validation checks

a) Corner surface points: Equation (1) describes the predictive model for computing the summed probability value (ProbValue) for a corner point, using variables A, C, and F as inputs. Fig. 16 presents a visual view of the extent to which the predicted values are well fitted to the actual probability values for the corner surface points.

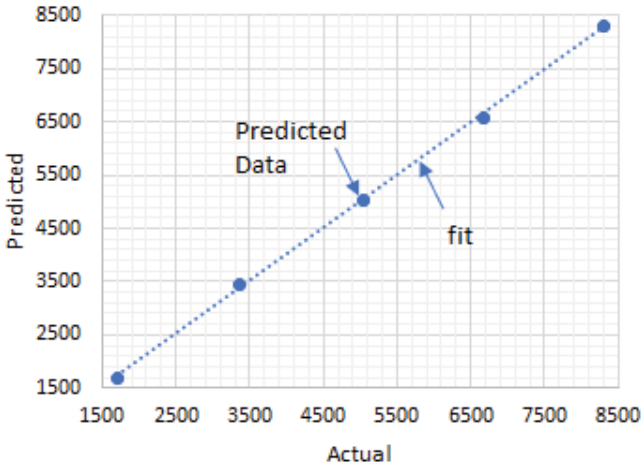

Fig. 15. A fit of the predicted versus actual PMCV for corner points

Fig. 16. Error histogram

$$ProbValue = k_0 + k_1 \times C^{11} + k_2 \times F^{0.85} \quad (1)$$

Where $k_0 = -461.24$, $k_1 = 5.6101 \times 10^{-17}$, and $k_2 = 305.341$.

b) Roof edge surface points: Equation (2) describes the predictive model for computing the summed probability value (ProbValue) for a roof edge surface point, using variables A, C, and F as inputs. Fig. 17 presents a visual view of the extent to which the predicted values are well fitted to the actual probability values for the roof edge surface points using the computed (2).

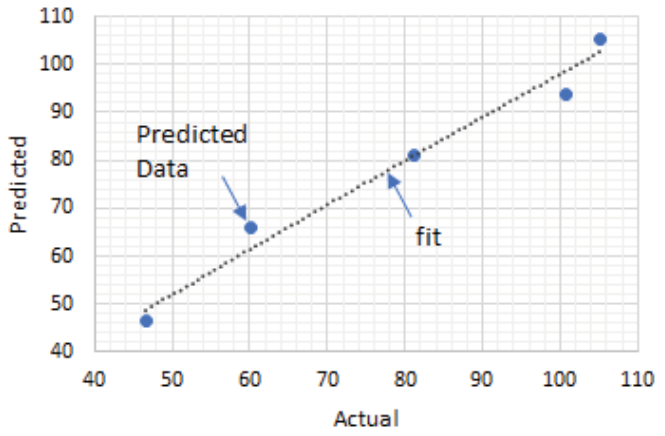

Fig. 17. A fit of the predicted versus the actual PMCV for roof edge points

$$\text{ProbValue} = j_0 + j_1 \times C^{4} + j_2 \times F^{2.4} + j_3 \times A^{0.93} \times C^{0.82} + j_4 \times A^{0.27} \times C^{1.2} \times F^{0.4} \quad (2)$$

Where $j_0 = 42.899$, $j_1 = -1.9446 \times 10^{-5}$, $j_2 = 0.01538$, $j_3 = -2.176 \times 10^{-14}$, and $j_4 = 5.862 \times 10^{-14}$.

c) Wall edge surface points: Equation (3) describes the predictive model for computing the summed probability value (ProbValue) for a wall edge surface point, using variables A, C, and F as inputs. Fig. 18 presents a visual view of the extent to which the predicted values are well fitted to the actual probability values for the roof edge surface points using (3).

$$\text{ProbValue} = m_0 + m_1 \times e^{2A} + m_2 \times C^{3.75} + m_3 \times e^{5F} + m_4 \times A^{-0.083} \times C^{4.8} + m_5 \times 2^{A} \times F^{-5.25} + m_6 \times C^{2.75} \times F^{0.01} + m_7 \times A^{-1.6} \times C^{10} \times F^{0.66} \quad (3)$$

Where $m_0 = 0.001029$, $m_1 = 2.7843 \times 10^{-51}$, $m_2 = 9.03 \times 10^{-6}$, $m_3 = 1.367 \times 10^{-112}$, $m_4 = -1.251 \times 10^{-7}$, $m_5 = -5.009 \times 10^{-10}$, $m_6 = -5.57 \times 10^{-5}$, and $m_7 = 4.199 \times 10^{-16}$.

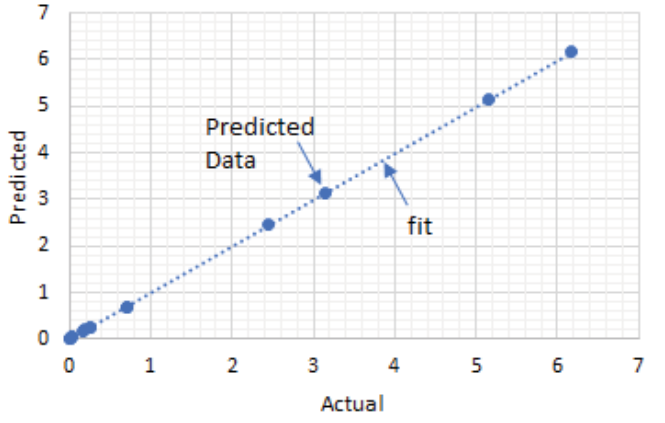

Fig. 18. A fit of the predicted versus the actual PMCV for wall edge points

d) Sidewall surface points: The summed probability of lightning strike to sidewall surface points can be estimated by (4), using variables A, C, and F as inputs. Fig. 19 presents a plot of the actual versus the predicted values.

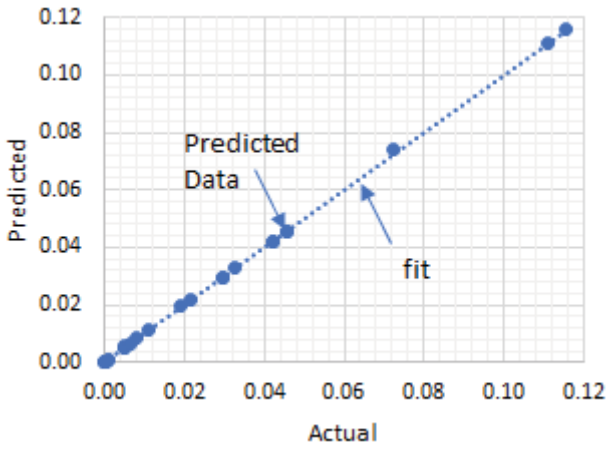

Fig. 19. A fit of the predicted versus the actual PMCV for sidewall points

$$\text{Pr}obValue = n_0 + n_1 \times A^{14} + n_2 \times C^{4.25} + n_3 \times F^{1.8} + n_4 \times A^{0.083} \times C^{0.69} + n_5 \times A^{15} \times F^{-3.3} + n_6 \times C^{2.05} \times F^{0.067} + n_7 \times A^{0.01} \times C^{1.6} \times F^{0.1} \quad (4)$$

Where $n_0 = -2.9218 \times 10^{-4}$, $n_1 = -4.0327 \times 10^{-27}$, $n_2 = -2.6635 \times 10^{-9}$, $n_3 = 3.5299 \times 10^{-7}$, $n_4 = 0.00036794$, $n_5 = 3.0598 \times 10^{-23}$, $n_6 = 0.00008559$, and $n_7 = -2.2560 \times 10^{-4}$.

e) Inner roof surface points: This is the inner part of the roof which are exposed to vertical lightning strikes from space points directly above this region. The cumulated probability of lightning strike to each inner roof surface point should be 1.0, but in the computation of the DEGM, the analysis was performed up to 300 m (not ∞) above the roof, and the resulting PMCV is 0.991. The value is constant for all inner roof surface points.

The value of the summed probability of lightning strike for each of the sidewalls and wall edge surface points are quite small in value, with some values in the order of 10^{-8}, and these small values were difficult to accurately predict by the model. The total PMCV for the whole structure is required to convert the results obtained using (1) to (4) to percentage values. A relationship between the probability of a corner point which was predicted accurately and the total sum of the probability of a lightning strike to all surface points on the four side faces of the cuboid structure (i.e. CubeSideP) was developed as shown in (5). The total probability of a strike to the four sides of the cuboid structures, even for the tallest 50 m high cuboids that have more side surface areas is typically less than 1.3% of the total probability, while surface points on the roof and corners account for the rest.

$$CubeSideP = z_0 + z_1 \times Corner_P^{3.8} + z_2 \times E^4 + z_3 \times G^{3.45} + z_4 \times \ln^4 F \quad (5)$$

Where $z_0 = 3.4407$, $z_1 = 6.681 \times 10^{-13}$, $z_2 = -4.4417 \times 10^{-14}$, $z_3 = 3.3648 \times 10^{-12}$, and $z_4 = -0.15141$.

CornerP is the probability of one corner surface point obtained using (1), E is the area of the roof in m^2, F is the height of the cube in m, and G is the total area of the four sides of the cuboid faces.

The total probability of a strike for the whole structure (i.e. the total PMCV) is the summation of the probability of a lightning strike for all the corner points, the wall edge points, roof edge points, the four sidewall points (i.e. CubeSideP), and the inner roof. This can be computed using (6), where L is the length and B is the breadth of the cuboid.

$$\text{Total PMCV} = 4 \times \text{CornerP} + (2L + 2B - 4) \times \text{Roof EdgeP} + (L-1) \times (B-1) \times 0.991 + \text{CubeSideP} \quad (6)$$

The percentage probability of a strike to a corner can then be determined by applying (7). Note that CornerP is calculated using (1).

$$\text{Corner Probability (\%)} = \frac{CornerP \times 100}{Total\ PMCV} \quad (7)$$

Likewise, the percentage probability of a strike to a point on the roof edge (RE) is defined by (8), and RoofEdgeP is obtained from (2).

$$\text{Roof Edge Probability (\%)} = \frac{RoofEdgeP \times 100}{Total\ PMCV} \quad (8)$$

In addition, the percentage probability of a strike to any surface point on the inner roof (IR) area of the cuboid structure is constant and can be obtained by (9).

$$\text{Inner Roof Probability (\%)} = \frac{0.991 \times 100}{Total\ PMCV} \quad (9)$$

Finally, for a side wall (SW) surface point, the probability of a strike may be estimated by (10), and SideWallP is obtained from (4).

$$\text{Side Wall Probability (\%)} = \frac{SideWallP \times 100}{Total\ PMCV} \quad (10)$$

Equations (1) to (10) were applied to compute the percentage probability of lightning strike to surface points on Cuboid A, and Cuboid B. Table II shows the result for few sample surface points in comparison with the actual value (Target).

The results from serial number 1 to 18 in Table II are from samples used in the development of the equations, and they are sourced from 10 m, 30 m, and 50 m high cuboids. To evaluate the ability of the model to predict results for new surface points, data samples from 20 m and 40 m cuboids, both for Cuboid A and Cuboid B, which were not part of the model development process were further analyzed. The results for the new samples are shown comparatively from serial number 19 to 30 in Table II. From the results, it is observed that the model was able to predict close results for samples used in developing the models, while for new data samples, there were slight deviations from the expected values.

TABLE II. COMPARISON OF THE PREDICTED RESULTS USING EQUATIONS WITH THE TARGET VALUE

SN	Cuboid Type	Point Type	Target	Indirect Equation (%)	Direct Equation (%)
1	A10	SW	0.00001	0.00001	–
2	A10	RE	0.29900	0.29901	0.29905
3	A10	C	10.91782	10.91819	10.91770
4	A30	IR	0.00288	0.00288	0.00295
5	A30	RE	0.23580	0.23580	0.23554
6	A30	C	14.65174	14.65165	14.65164
7	A50	SW	0.00008	0.00008	–
8	A50	RE	0.20343	0.20343	0.20360
9	A50	C	16.05324	16.05349	16.05312
10	B10	IR	0.00705	0.00705	0.00709
11	B10	RE	0.33125	0.33125	0.33115
12	B10	C	12.09545	12.09554	12.09533
13	B30	SW	0.00010	0.00010	–
14	B30	RE	0.25201	0.25201	0.25231
15	B30	C	15.65919	15.65903	15.65910
16	B50	C	16.94614	16.94634	16.94602
17	B50	SW	0.00000	0.00000	–
18	B50	RE	0.21474	0.21474	0.21452
19	A20	WE	0.00097	0.00101	–
20	A20	C	13.32972	13.93628	13.78360
21	A20	RE	0.26071	0.24414	0.24524
22	A40	SW	0.00007	0.00007	–
23	A40	RE	0.21777	0.22998	0.22135
24	A40	C	15.48832	15.03512	16.34327
25	B20	C	14.41524	15.02727	14.85685
26	B20	SW	0.00005	0.00005	–
27	B20	RE	0.28195	0.26325	0.26719
28	B40	IR	0.00244	0.00241	0.00453
29	B40	RE	0.23105	0.24459	0.23474
30	B40	C	16.43327	15.99009	16.33579

Further, an equation for directly predicting the percentage probability (Target) of a lightning strike to the roof edge, corner, and inner roof area was developed. The sidewall and the wall edges were excluded from the analysis because of their small strike probability which reduces the accuracy of a general

equation for all the five types of points. The result is directly in percentage using (11), and this is an alternative to the indirect analysis by calculating PMCV. The equation is only for RE, IR, and C point types, and it applies A, B, C, D, and E as input variables.

$$\text{Target } (\%) = Q_1 + Q_2 + Q_3 + Q_4 \tag{11}$$

Where Q_1, Q_2, Q_3, and Q_4 are defined as follows, and $t_0 = -8.6018$, $t_1 = 9.838205$, $t_2 = -27.930$, $t_3 = 0.0001855$, $t_4 = 0.0012095$, $t_5 = 2.1612 \times 10^{-11}$, $t_6 = -0.088903$, $t_7 = -4.351 \times 10^{-16}$, $t_8 = 1.2513 \times 10^{-7}$, $t_9 = 379.82078$, $t_{10} = -0.08143$, $t_{11} = 9.097 \times 10^{-9}$, $t_{12} = 6.811 \times 10^{-12}$, $t_{13} = -0.34028$, $t_{14} = -2.398 \times 10^{-8}$, $t_{15} = -1.8685 \times 10^{-5}$, $t_{16} = 185702.9$, $t_{17} = -1.466 \times 10^{-4}$, $t_{18} = -4.4026 \times 10^{-20}$, and $t_{19} = 2.242 \times 10^{-15}$.

$$Q_1 = t_0 + t_1 \cdot B^{0.24} + t_2 \times C^{-2} + t3 \times D^{5.9} + t_4 \times E^{0.96} + t_5 \times A^{2.95} \times B^{3.25} + t_6 \times A^{3.35} \times 6^{-C} + t_7 \times A^5 \times D^4$$

$$Q_2 = t_8 \times A^{1.55} \times E^{0.22} + t_9 \times B^{0.32} \times C^{-3.2} + t_{10} \times B^{0.77} \times E^{0.18} + t_{11} \times C^{-5.25} \times D^{16} + t_{12} \times C^{3.55} \times E^{0.44} + t_{13} \times \ln^3 D \times E^{0.167}$$

$$Q_3 = t_{14} \times A^{1.1} \times B^{4.8} \times C^{-2.75} + t_{15} \times B^{0.97} \times C^{3.4} \times D^{-4.9} + t_{16} \times C^{-0.125} \times D^{-5.55} \times E^{-0.65} + t_{17} \times A^{0.09} \times B^{-4.9} \times C^{2.75} \times 7^{-D}$$

$$Q_4 = t_{18} \times B^{-2.8} \times C^{0.07} \times D^{-1.45} \times E^6 + t_{19} \times A^{0.27} \times B^{2.75} \times C^{-2.5} \times D^{0.8} \times E^{3.25}$$

A comparison of the predictions from both the ANN and equation-based models shows that the ANN model performed far better in terms of predictive accuracy for new samples. This can be attributed to the ability of the artificial neural network to determine and assign appropriate path weights to neural inputs to ensure they significantly depict the relationship between the input dataset and the target output.

VI. Conclusion

Accurate design of lightning protection systems (LPS) is vital for ensuring the safety of lives and properties, and the performance integrity of the LPS. Air-termination networks must be positioned at high-risk points on a structure to ensure optimal lightning interception. The dynamic electro-geometrical model; a technique for analyzing the probability of lightning strikes to different points on a structure requires computer programming and takes time to compute, and these may be challenging for LPS design engineers to quickly apply. Alternative approaches using artificial neural networks and equations developed using data fitting techniques were explored in this study. A 7-input neural network model was developed using a two-layer feed-forward network comprising of 18 neurons. The ANN model was trained with data obtained from simulated DEGM analysis of cuboid structures of different dimensions. The result shows close approximations to expected result with an overall regression R^2 of 1. In terms of the ability of the models developed to predict accurate results for unfamiliar data samples, the ANN model performed far better than the equation-based model in predicting results for surface points on new cuboid structures.

Acknowledgment

This is to appreciate the support of the Nigerian Petroleum Technology Development Fund (PTDF) through the Overseas Scholarship Scheme in partnership with the German Academic Exchange Service (DAAD).

References

[1] V. Rakov, A. Borghetti, C. Bouquegneau, W. Chisholm, V. Cooray, K. Cummins, et al., "CIGRE technical brochure on lightning parameters for engineering applications," in 2013 International Symposium on Lightning Protection (XII SIPDA), pp. 373-377, 2013.

[2] V. Zimackis and S. Vitolina, "Advancements in building lightning protection zone estimation," in 2015 IEEE 5th International Conference on Power Engineering, Energy and Electrical Drives (POWERENG), pp. 211-214, 2015.

[3] F. D'Alessandro, "Striking distance factors and practical lightning rod installations: a quantitative study," Journal of Electrostatics, vol. 59, pp. 25-41, 2003.

[4] S. Grzybowski and T. Disyadej, "Laboratory investigation of lightning striking distance to rod and transmission line," in 2010 Asia-Pacific International Symposium on Electromagnetic Compatibility, pp. 1301-1304, 2010.

[5] Z. Flisowski and P. Sul, "Individual assessment of the lightning hazard of building objects as a guarantee of their proper protection," Electric Power Systems Research, vol. 178, 2020.

[6] A. Srivastava and M. Mishra, "Positioning of lightning rods using Monte Carlo technique," Journal of Electrostatics, vol. 76, pp. 201-207, 2015.

[7] I. Ullah, M. N. R. Baharom, H. Ahmad, F. Wahid, H. M. Luqman, Z. Zainal, et al., "Smart Lightning Detection System for Smart-City Infrastructure Using Artificial Neural Network," Wireless Personal Communications, vol. 106, pp. 1743-1766, 2019.

[8] A. I. Adekitan and M. Rock, "A further look at dynamic electro-geometrical model: Its fundamentals and implementation," Ain Shams Engineering Journal, 2020.

[9] A. Kern and R. Brocke, "Planning of Air-Termination Systems with the Dynamic Electro-Geometrical Model – Possible Practical Applications," presented at the 10th Asia-Pasific International Conference on Lightning, Krabi Resort, Thailand, 2017.

[10] M. Ahmadi, H. Naderpour, and A. Kheyroddin, "ANN model for predicting the compressive strength of circular steel-confined concrete," International Journal of Civil Engineering, vol. 15, pp. 213-221, 2017.

[11] E. T. Lau, L. Sun, and Q. Yang, "Modelling, prediction and classification of student academic performance using artificial neural networks," SN Applied Sciences, vol. 1, p. 982, 2019.

[12] M. M. Saritas and A. Yasar, "Performance Analysis of ANN and Naive Bayes Classification Algorithm for Data Classification," International Journal of Intelligent Systems and Applications in Engineering, vol. 7, pp. 88-91, 2019.

[13] G. Villarrubia, J. F. De Paz, P. Chamoso, and F. D. la Prieta, "Artificial neural networks used in optimization problems," Neurocomputing, vol. 272, pp. 10-16, 2018.

[14] Aderibigbe Israel Adekitan, B. Adetokun, and K. Okokpujie, "A data-based investigation of vehicle maintenance cost components using ANN," IOP Conference Series: Materials Science and Engineering, vol. 413, p. 012009, 2018.

[15] T. Hossen, S. J. Plathottam, R. K. Angamuthu, P. Ranganathan, and H. Salehfar, "Short-term load forecasting using deep neural networks (DNN)," in 2017 North American Power Symposium (NAPS), pp. 1-6, 2017.

[16] Z. Zhang, "Artificial Neural Network," in Multivariate Time Series Analysis in Climate and Environmental Research, Z. Zhang, Ed., ed Cham: Springer International Publishing, pp. 1-35, 2018.

[17] SigmaLab. (2019). Available: https://www.ndcurvemaster.com/